CDKZM

CRNOGORSKO DRUŠTVO ZA KOROZIJU, ZAŠTITU MATERIJALA I ZAŠTITU ŽIVOTNE SREDINE

PETI MEĐUNARODNI SIMPOZIJUM O KOROZIJI I ZAŠTITI MATERIJALA, ŽIVOTNOJ SREDINI I ZAŠTITI OD POŽARA

KNJIGA RADOVA

FIFTH INTERNATIONAL SYMPOSIUM ON CORROSION AND MATERIALS PROTECTION, ENVIRONMENTAL PROTECTION AND PROTECTION AGAINST FIRE

PROCEEDINGS

Bar, 26-29. septembar 2023. godine

POKROVITELJ

Opština Bar

SPONZORI

Metalurško-tehnološki fakultet Podgorica
WR Dynamic Company d.o.o- Kotor
Čelebić d.o.o. Podgorica
Tujko d.o.o. Kotor
Poliex a.d. Berane
Institut za razvoj i istraživanja u oblasti zaštite na radu Podgorica
Hemosan d.o.o. Bar
Megaplast d.o.o. Podgorica

Izdavač
CRNOGORSKO DRUŠTVO ZA KOROZIJU,
ZAŠTITU MATERIJALA I ZAŠTITU ŽIVOTNE SREDINE

Urednik
Prof. dr Darko Vuksanović

CIP - Каталогизација у публикацији
Национална библиотека Црне Горе, Цетиње

ISBN 978-9940-9334-4-9
COBISS.CG-ID 27476484

S A D R Ž A J
C O N T E N T

PLENARNA PREDAVANJA

PRENARY LECTURES

Novel Immunomodulatory and Anti-inflammatory Nano Amorphous Calcium Phosphate@Chitosan Oligolactate coatings on titanium substrate for potential medical and dental use

Miroslav M. Pavlović[1,2], Marijana R. Pantović Pavlović[1,2]
[1]*Department of Electrochemistry, Institute of Chemistry, Technology and Metallurgy, National Institute of the Republic of Serbia, University of Belgrade, 11000 Belgrade, Serbia*
[2]*Center of Excellence in Chemistry and Environmental Engineering—ICTM, University of Belgrade, 11000 Belgrade, Serbia*

Abstract:

Background: Titanium (Ti) is widely used in medical and dental implants. Calcium phosphate (CPs) coatings enhance Ti implants' osteoinductive properties, and additives further improve these coatings. Recently, a nano amorphous calcium phosphate (nACP) coating decorated with chitosane oligolactate (ChOL) and selenium (Se) showed immunomodulatory effects. This study investigates the surface morphology, composition, bioactivity, mechanical properties, and Se release mechanism of the nACP/ChOL/Se hybrid coating on Ti substrates. Amorphous calcium phosphate (ACP) was synthesized, and the ACP/ChOL/Se hybrid coating was deposited on Ti substrates using in situ anaphoretic deposition. Surface morphology was analyzed using SEM, AFM, XRD, and FTIR. The distribution of Se within the coating was examined with EDS. Bioactivity was evaluated in simulated body fluid (SBF), and adhesion was tested using a scratch test method. In vitro testing determined the release mechanism of Se. SEM images illustrated the surface morphology, while AFM provided a detailed analysis of surface roughness. XRD analysis revealed structural and phase composition, and EDS confirmed Se distribution within the coating. The coating exhibited bioactivity in SBF and showed good adhesion according to the scratch test. In vitro testing uncovered the release mechanism of Se from the coating. This study successfully characterized the surface morphology, composition, bioactivity, and Se release mechanism of the nACP/ChOL/Se hybrid coating on Ti substrates, offering insights for developing immunomodulatory coatings for medical and dental applications.
Keywords: *deposition; hybrid coating; ion release; implants; inflammatory mediators; nano calcium phosphate*

1. Introduction

Thus far, titanium (Ti) has been widely utilized as a material for creating diverse implants in the field of medicine and dentistry [1]. The addition of hydroxyapatite (HAp) coatings to titanium (Ti) substrates has proven to be

highly effective in enhancing the osteoinductive properties of these implants, making them suitable for use in dentistry and medicine [2]. When jaw bone fixation is performed using HAp-coated Ti implants, a close bond is formed between the implant and the surrounding bone tissue, with no presence of other tissue in the interlayer [3]. The incorporation of nanostructured hydroxyapatite (nHAp) and similar calcium phosphates (CP) as coatings on Ti implants has further improved their properties, facilitating the earlier formation of new bone tissue [4]. Moreover, amorphous calcium phosphates (ACPs), which undergo a transformation into more stable structures like HAp, have demonstrated significant potential in the realm of reconstructive medicine [5].

In the quest to address implant-associated infections (IAIs), particularly in the case of titanium (Ti) implants, a range of strategies has been developed to effectively reduce IAIs [6,7]. One approach involves incorporating silver (Ag) into hydroxyapatite (HAp) coatings, resulting in the creation of a coating with antibacterial properties [8]. Furthermore, researchers have explored the antibacterial effects of Ti-coated HAp doped with various elements such as yttrium (Y), copper (Cu), and strontium (Sr) [9–11]. The presence of strontium (Sr), magnesium (Mg), and zinc (Zn) ions in HAp-based coatings has also demonstrated the ability to enhance their antibacterial properties [12].

In addition to ion doping in HAp, antibacterial properties can be achieved by employing hybrid coatings composed of HAp and polymers on titanium surfaces. Chitosan (Ch) and its derivatives, known for their excellent biocompatibility, non-toxicity, and favorable physical and chemical properties, possess remarkable antibacterial capabilities [13]. Micro-nanostructured HAp/chitosan (HAp/Ch) coatings on titanium substrates have shown the ability to inhibit the growth of various bacteria while simultaneously enhancing the coating's bioactivity potential [14]. Moreover, multifunctional coatings combining nano amorphous calcium phosphate (nACP) and chitosan oligosaccharide lactate (ChOL) have exhibited notable bioactive properties [15]. To ensure strong adhesion of nACP@ChOL coatings on titanium, a successful approach involves employing the simultaneous technique of anodization and anaphoretic electrodeposition [16].

Electrodeposition techniques have proven effective not only for depositing HAp/chitosan (HAp/Ch) coatings on titanium but also for incorporating antibiotics into these coatings [17]. Besides biocompatibility and mechanical properties, enhancing the bioactivity of HAp- or ACP-based coatings in conjunction with chitosan is crucial for their application in medicine and dentistry. The addition of cellulose acetate (CA) to nHAp/Ch-based coatings has demonstrated a significant improvement in bioactivity [18]. Additionally, the bioactivity of HAp/Ch-based coatings has been enhanced through the incorporation of carbon nanotubes and graphene during the electrodeposition process [17,19].

In addition to the previously discussed properties of nACP@ChOL and nHAp@ChOL coatings on titanium (Ti), which are crucial for their potential applications, the response of the body and organism after implantation represents a property of utmost importance. Generally, the introduction of a foreign object into the body of a mammal triggers complex biochemical processes that may lead to inflammation, infection, and other reactions [20]. Ongoing research in the field of HAp coatings on Ti substrates aims to develop coatings with properties that can reduce or completely inhibit the adverse response of the organism following implantation. In addition to essential properties such as biocompatibility, bioactivity, antibacterial properties, and corrosion stability, the latest generation of Ti coatings is also focused on their immunomodulatory properties. The design of biomaterials and coatings with anti-inflammatory characteristics presents a significant challenge for researchers today [21].

Studies have explored the incorporation of nonsteroidal anti-inflammatory drugs (NSAIDs) as part of HAp coatings on Ti substrates, and the results have shown no negative impact on the osseointegration of such implants while providing anti-inflammatory effects [22,23]. Furthermore, the addition of resveratrol to the HAp@Ch system has demonstrated simultaneous promotion of osteo-differentiation and significant anti-inflammatory effects during in vitro testing [24]. In our recent research, we have developed a nACP@ChOL-based coating decorated with selenium (Se) on Ti using the anodization/anaphoretic electrodeposition process [25]. The focus of these studies was to investigate the immunomodulatory properties of the nACP@ChOL coatings decorated with Se on Ti in living systems, specifically in vivo. The nACP@ChOL-Se coating has shown an increase in the Arg1 (arginase 1) ratio and M2/M1 (M2 macrophages/M1 macrophages) following implantation in a living organism, indicating its beneficial effect on the immune response.

The current study aims to investigate the surface morphology and specific characteristics of the nACP@ChOL coating decorated with selenium (Se) on titanium (Ti) substrates. During the electrodeposition process of nACP, its transformation into nanostructured hydroxyapatite (nHAp) takes place. X-ray structural analysis was employed to examine the coating’s phases. The distribution of Se within the coating was analyzed using the suitable technique of Energy-Dispersive X-ray Spectroscopy (EDS). Furthermore, the potential bioactivity of the coating was evaluated in a simulated body fluid (SBF) environment. To assess the mechanical properties essential for potential applications and adhesion to the substrate surface, the Scratch test method was employed. Additionally, in vitro testing at a temperature of 37°C was conducted to determine the release mechanism of Se into the surrounding environment during potential applications.

2. Materials and Methods

Amorphous calcium phosphate (ACP) was synthesized by rapidly adding 150 mL of a 26.6% mass solution of $Ca(NO_3)_2$ in double-distilled water to 400 mL of an $(NH_4)_3PO_4$ solution. The later was prepared by combining 7 mL of H_3PO_4, 165 mL of NH_4OH, and 228 mL of double-distilled H_2O. The resulting solution was continuously stirred at 100 rpm and 50°C for 60 minutes. The obtained fine gel was aged for 15 seconds before being collected, rinsed with water, and centrifuged at 4000 rpm in a Hettich Universal 320 centrifuge at 5°C for 1 hour. The resulting precipitate was freeze-dried at -30°C and a pressure of 0.37 bar for 1 hour, followed by a final drying step at -40°C and a pressure of 0.12 bar for 2 hours.

For the in situ anaphoretic deposition processes of ACP/ChOL/Se hybrid multifunctional composite coatings on Ti substrates, 99.7% pure titanium plates (ThermoFisher) with dimensions of (20 × 10 × 0.89) mm were utilized. The titanium plates underwent precoating preparation which included sanding with silicon carbide (SiC) sandpaper with grit sizes of 600, 1000, 2000, and 3000, followed by polishing using alumina with grain sizes of 1, 0.3, and 0.05 µm (Buehler, IL, USA). Subsequently, all samples were washed and purified in 96% ethanol (Sigma Aldrich, Taufkirchen, Germany) using an ASONIC PRO 50 ultrasonic cleaner (ASonic, Ljubljana, Slovenia) with a power of 120 W and a frequency of 40 kHz for 30 minutes. To prevent spontaneous oxidation, the samples were stored in ethanol prior to deposition.

The ACP/ChOL/Se hybrid coatings on Ti substrates were obtained through in situ anaphoretic precipitation from an appropriate ethanolic suspension. To prepare the suspension, 273.5 mg of Na_2SeO_3 (equivalent to a total of 125 mg Se, Sigma Aldrich, Taufkirchen, Germany) was added to 50 mL of double-distilled water and stirred for 5 minutes until completely dissolved. Next, 125 mg of chitosan oligosaccharide lactate (ChOL, Mw 5000, Sigma Aldrich, Taufkirchen, Germany) was added to the same solution, and the mixture was continuously stirred at 300 rpm overnight using a rotary magnetic stirrer. The total amount of selenium (125 mg) and a ChOL:Se mass ratio of 1:1 were selected as being continuation of the previous research [25]. After the ChOL had swelled and dissolved overnight, 50 mL of 96% ethanol and 1.000 g of ACP were added to the solution, followed by stirring at 300 rpm for another overnight. The pH was adjusted using 5 mL of 1 M NaOH to enhance the suspension's stability for subsequent anodization/anaphoretic deposition. The suspension was continuously mixed on a rotary magnetic stirrer at 300 rpm to ensure particle homogenization and maintain a stable suspension throughout the deposition process. The in situ anaphoretic deposition was performed using a custom-made two-electrode electrochemical cell, with the titanium plate (20 × 10 × 0.89) mm serving as the anode and a pair of 316 grade stainless steel plates (20 × 10 × 0.89) mm as the cathode, placed parallel to the anode at a

distance of 10 mm. The ACP/ChOL/Se hybrid coatings on titanium were deposited at a constant voltage of 60 V for 1 minute, followed by air-drying for 24 hours at 25°C.

The surface morphology of the hybrid coatings was analyzed using field-emission scanning electron microscopy (Tescan Mira 3 XMU FEG-SEM). EDS analysis was conducted using a Jeol JSM 5800 SEM with a SiLi X-ray detector (Oxford Link Isis series 300, Abingdon, UK). The composite samples were subjected to X-ray diffraction (XRD) analysis for structural and phase evaluation. The measurements were carried out using a Philips PW 1050 powder diffractometer (Malvern Panalytical Ltd, Malvern, UK) at room temperature. Ni-filtered Cu Kα radiation (λ = 1.54178 Å) and a scintillation detector were used within the 2θ range of 3–82° with a scanning step size of 0.02°. The scanning rate was set at 5 seconds per step. Phase analyses were conducted using EVA V.9.0 software. To assess the adhesion of the coatings, the ASTM D 3359-02 Standard Test Methods for Measuring Adhesion by Tape, cross-cut tape test (B), was performed. The adhesion measurements were recorded using a camera equipped with a Leica 20 MP Ultra Wide Angle Lens and an aperture of f/2.2.

The surface characteristics of the polymer composites were analyzed using a contact mode atomic force microscope (AFM) "Nanoscope III" AFM Multi Mode Scanning Probe Microscope manufactured by "Digital Instruments" (Munich, Germany). The obtained microscopy data were processed using the NanoScope Analysis software.

The concentration of selenium (total, in all oxidation states present in the coating and released to SBF solution) was measured using the inductively coupled plasma optical emission spectrometry (ICP-OES) analytical technique. ICP-OES measurements were performed on an iCAP 6500 Duo ICP instrument (Thermo Fisher Scientific, Cambridge, UK) with iTEVA operating software. The samples were introduced into the plasma by direct liquid aspiration. Calibration standard solutions in the appropriate concentration range (1-50000 µg/L) were prepared from a certified standard solution: Selenium, plasma standard solution, Specpure®, Se 1000 µg/ml (Alfa Aesar GmbH & Co KG, Germany). The correlation coefficient for selenium was >0.99. Selenium quantification was performed at the emission wavelength of Se I 196.090 nm. The concentration measurements were repeated three times (n=3). The relative standard deviation of the repeated measurements was RSD < 0.5%. For determination of total Se content in the hybrid coating, the coating was dissolved in aqua regia (HCl + HNO_3, 3:1 v/v) by boiling. The titanium plate remained intact and undissolved. After complete dissolution of the entire coating, the solution was quantitatively transferred to a volumetric flask with a capacity of 25 mL and diluted to the marked volume. The concentration of selenium in the resulting solution was measured using the ICP-OES analytical technique.

Michelson MB Series Bomen Fourier transform infrared spectroscope (FTIR) spectroscope (Hartmann Braun, Munich, Germany) was used to conduct FTIR analysis. The FTIR measurements were carried out in the wavenumber range of 400 to 4000 cm^{-1} with a spectral resolution of 0.5 cm^{-1}.

3. Results

3.1. Hybrid ACP/ChOL/Se coating characterization

To characterize the physical appearance and surface area of the synthesized hybrid ACP/ChOL/Se coatings on titanium substrates, SEM imaging was employed. Figure 1 depicts the ACP/ChOL/Se hybrid coating prepared by in situ anodization/anaphoretic deposition process, which was performed for 1 minute, which is the same as in our previous research [25].

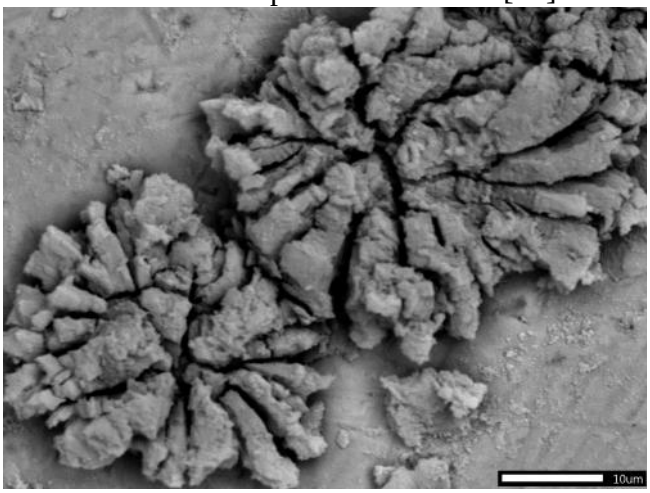

Figure 1. SEM images of ACP/ChOL/Se hybrid coating on titanium substrate deposited by in situ anodization/anaphoretic deposition process at 60 V of the hybrid coating.

Figure 2 shows two -dimensional AFM pictures with surface morphology and linear roughness analysis of the ACP/ChOL/Se hybrid coating surface.

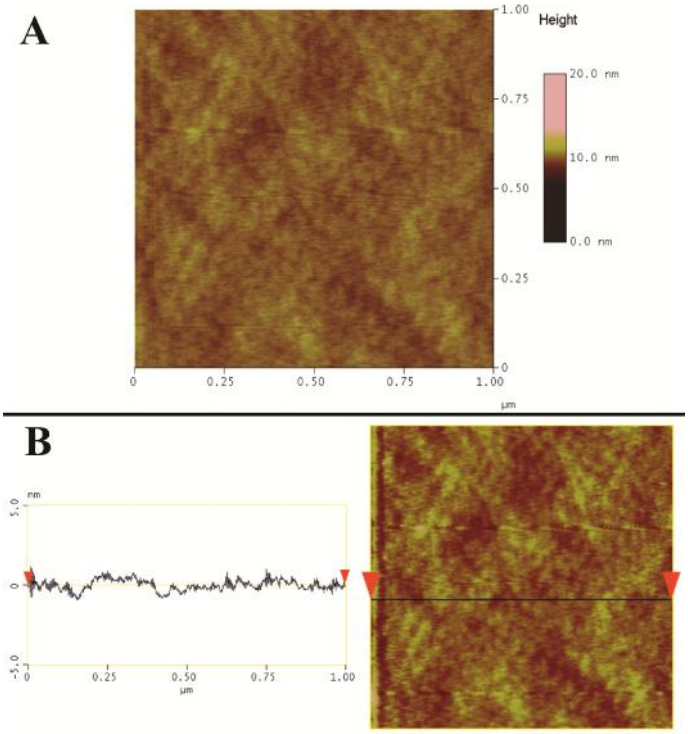

Figure 2. (A) Two-dimensional AFM image of the ACP/ChOL/Se hybrid coating surface and (B) linear roughness analysis (root mean square - RMS) of the same coating

The EDS area analysis results, presented in Figure 3 through EDS mapping, provided confirmation of the presence of building constituents, namely titanium (Ti), oxygen (O), calcium (Ca), phosphorus (P) and selenium (Se), in the ACP/ChOL/Se hybrid coating on titanium substrate.

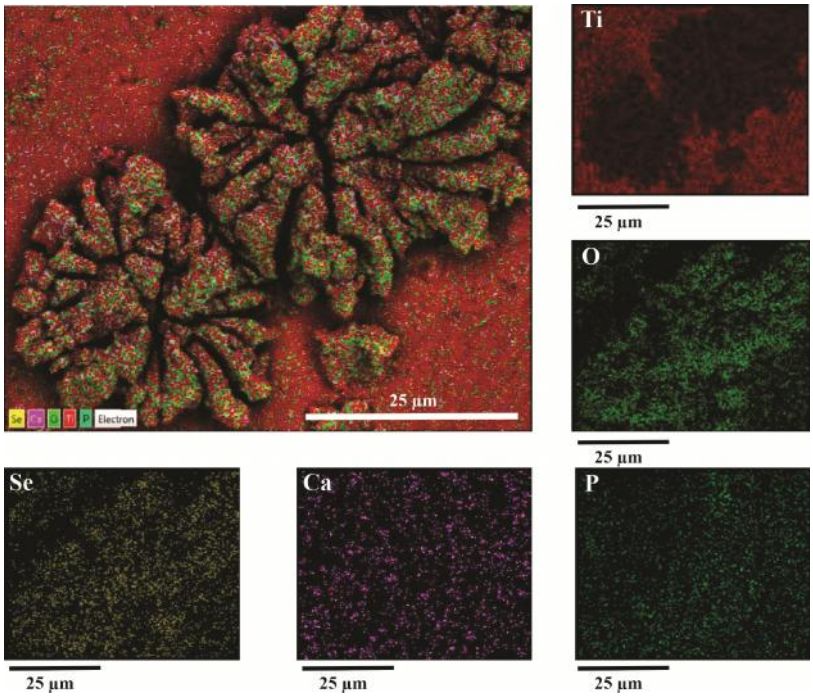

Figure 3. EDS mapping of ACP/ChOL/Se hybrid coating on titanium substrate with all ions distribution and distribution of titanium (Ti), oxygen (O), selenium (Se), calcium (Ca) and phosphorus (P).

Figure 4 displays the XRD diffraction pattern of ACP/ChOL/Se hybrid coating on the titanium substrate.

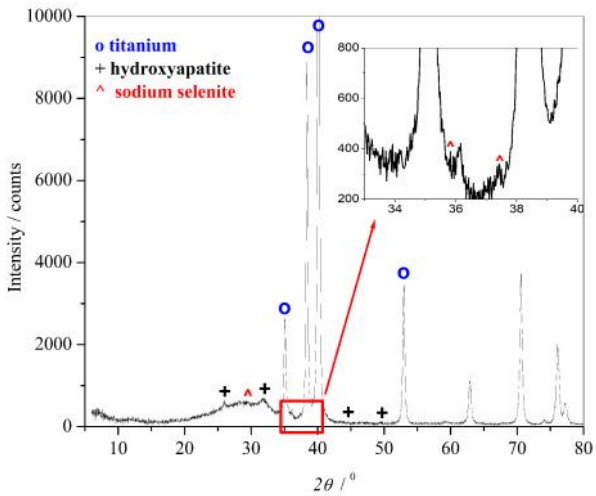

Figure 4. XRD diffractogram of ACP/ChOL/Se hybrid coating on titanium substrate deposited by in situ anodization/anaphoretic deposition process at 60 V after 1 min of deposition with enlarged portion of the spectrum from 2Θ=32° to 40°.

The optical images of the ACP/ChOL/Se hybrid coating on titanium substrate before and after performing adhesion testing, quantified by adhesion test according to ASTM D 3359-02: Standard Test Methods for Measuring Adhesion by Tape; cross-cut tape test (B), are shown in Figure 5.

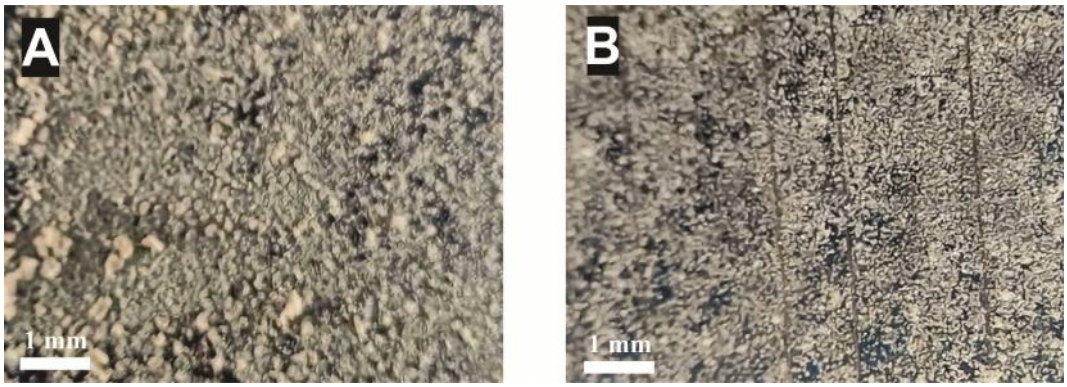

Figure 5. Optical image of the ACP/ChOL/Se hybrid coating on titanium substrate obtained at 60 V (A) before and (B) after performing adhesion testing according to ASTM D 3359-02.

3.2. Bioactivity

To evaluate the bioactivity of the composite coatings, the ACP/ChOL/Se hybrid coatings on titanium substrate were subjected to immersion in SBF solution and analyzed at different time intervals. The surface morphologies of the hybrid composites after immersion in the SBF solution are presented in Figure 6 (namely, Figure 6A and 6B after 3 days of immersion and Figures 6C and 6D after 10 days of immersion).

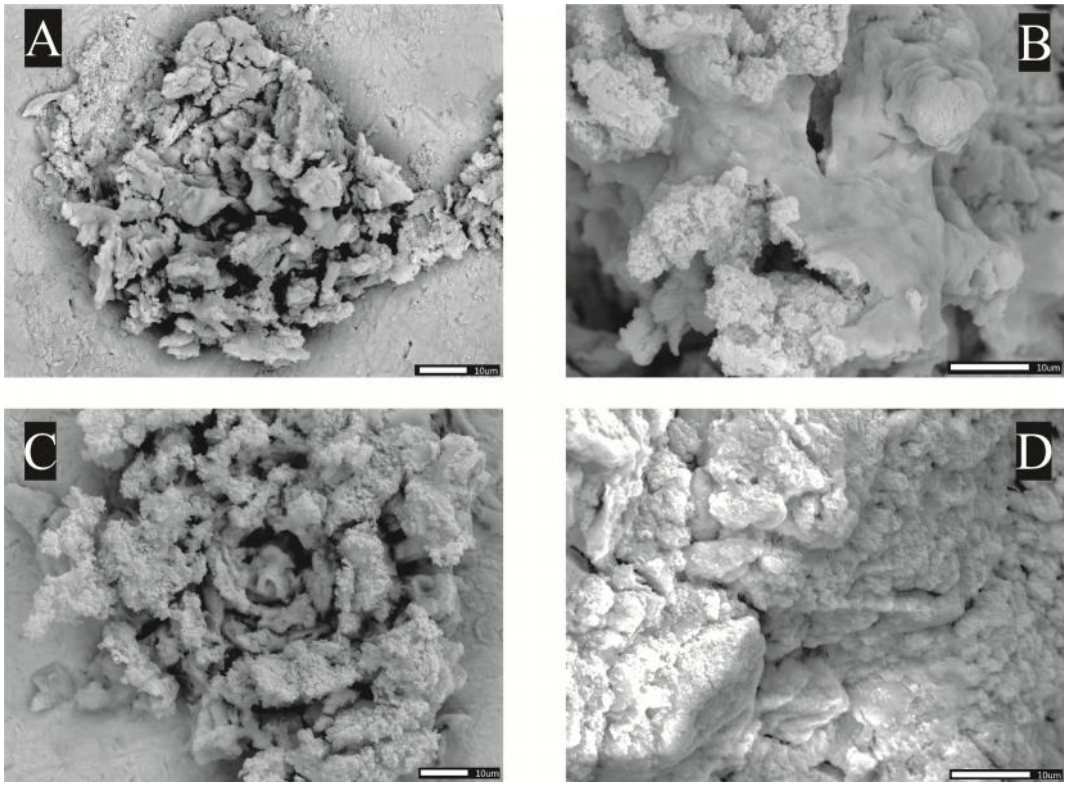

Figure 6. (A) and (B) SEM micrographs of the ACP/ChOL/Se hybrid coatings on a titanium substrate after immersion in the SBF solution for 3 days. (C) and (D) SEM micrographs of the coatings after 10 days of immersion in the SBF solution.

Figure 7 shows the EDS mapping analysis results of the ACP/ChOL/Se hybrid coatings after immersion in SBF for 10 days.

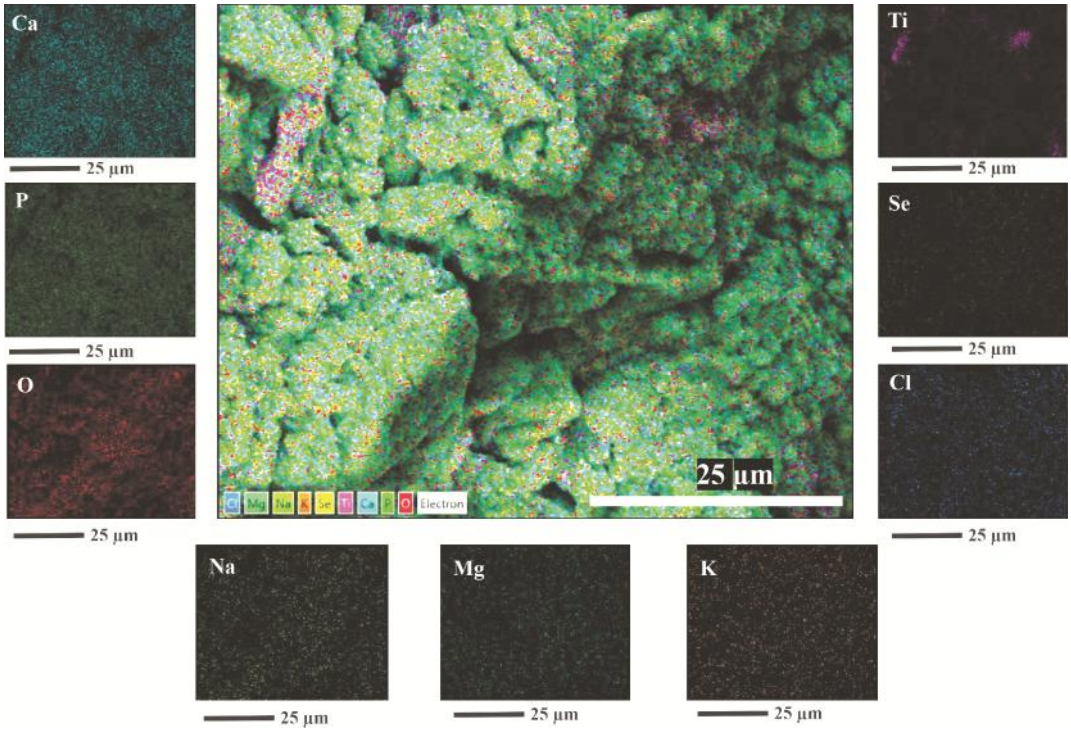

Figure 7. EDS mapping of ACP/ChOL/Se hybrid coating on titanium substrate with all ions distribution and distribution of titanium (Ti), oxygen (O), selenium (Se), calcium (Ca), phosphorus (P), Sodium (Na), magnesium (Mg), potassium (K) and chloride (Cl).

The FTIR spectra of the ACP/ChOL/Se hybrid coatings before and after 10 days immersion in SBF are presented in Figure 8. The changes in the peaks' intensities, as well as appearances or disappearances of the peaks are labeled with numbers, which is discussed in the Discussion section.

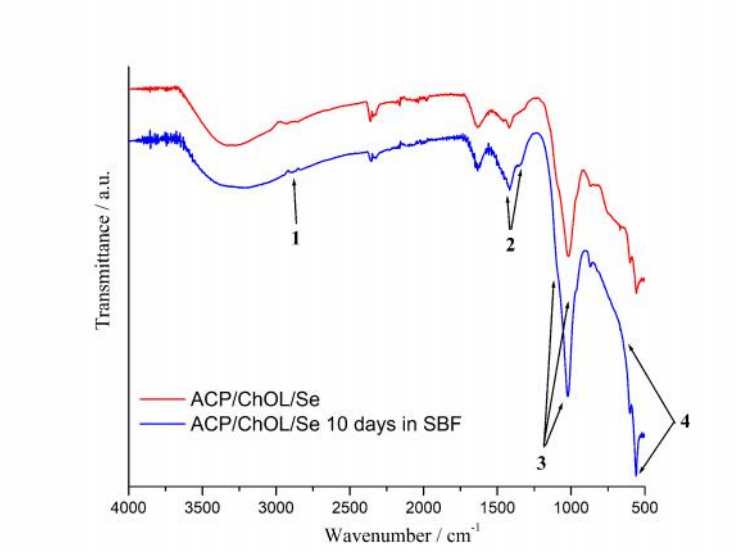

Figure 8. FTIR spectra of ACP/ChOL/Se hybrid coatings on titanium substrate before and after 10 days immersion in SBF.

3.3. Ion release study

The results of our previous research [25] have unequivocally confirmed that the ACP/ChOL/Se multifunctional hybrid composite coating on a titanium substrate has the immunomodulatory and anti-inflammatory effect compared to the pure grade 2 titanium implants. However, it was of the utmost importance to investigate the Se-release mechanism in vitro. The results of the investigation of selenium release in SBF medium is shown in Figure 9.

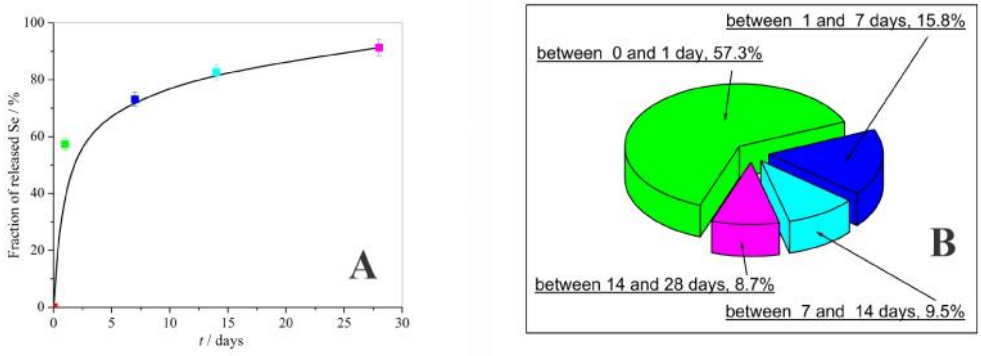

Figure 9. (A) Cumulative curve of the release of selenium in SBF medium at 37°C over the investigated time period and (B) release of selenium in percents over the investigated period: relative review

3.4. In vivo study

To examine the effect of novel coating on biocompatibility, we did not use the traditional approach (histological examination) but decided to examine functional aspects in the tissue around the implant that might give better insight into the presence of inflammation (proinflammatory cytokines' gene expression), M1 macrophages (iNOS), M2 macrophages (Arg1), fibrous capsule formation (TGF-β) and vascularization (VEGF).
ACP/ChOL/Se coating of titanium implants does not affect the general physical condition of animals, and there was no evidence of redness, swelling, or infection around implanted disks. Examination of macrophage functional polarization showed a similar presence of M1 macrophages (iNOS expression) (Figure 10A) at earlier time points, but lower at day 28 post-implantation in the tissue around ACP/ChOL/Se implants. Additionally, a higher level of M2 polarization (Arg1 expression) (Figure 10B) was noted at all time points examined, resulting in a higher M2/M1 macrophage ratio (Figure 10C) in ACP/ChOL/Se coated implants compared to pure titanium implants. Lower inflammation measured by gene expression of proinflammatory cytokines IL-1β (Figure 10D) and TNF (Figure 10E) was noted in presence of ACP/ChOL/Se implants at all time points examined. In contrast to IL-1β and TNF, a transiently higher IL-6 expression (solely at day 7 post-implantation) (Figure 10F) was observed in ACP/ChOL/Se implants. The tissue surrounding ACP/ChOL/Se implants was characterized by a lower expression of TGF-β (Figure 10G) at all time points post-implantation, while no differences were detected in VEGF expression (Figure 10H).

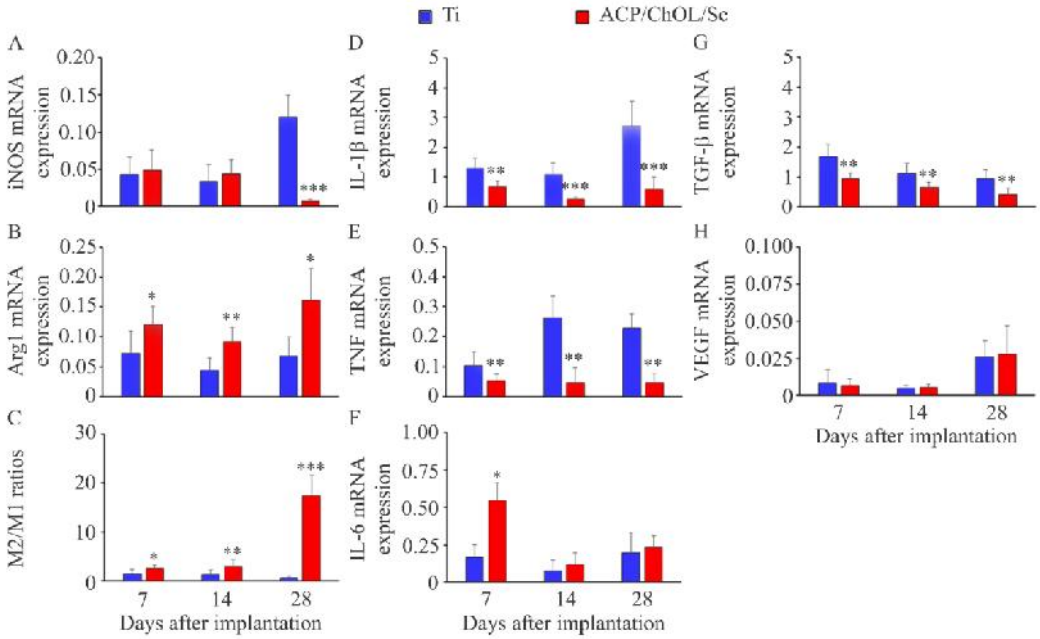

*Figure 10. Gene expression in tissue surrounding pure titanium or ACP/ChOL/Se coated titanium disks following subcutaneous implantation in rats evaluated by RT-PCR analysis. (A) mRNA expression of M1 macrophage marker iNOS. (B). mRNA expression of M2 macrophage marker Arg1. (C) M2/M1 ratio calculated as Arg1/iNOS. mRNA expression of IL-1β (D), TNF (E), IL-6 (F), TGF-β (G) and VEGF (H). Data are presented as mean ± standard deviation from 8 animals per group per time point. Statistically significant differences at: * $p < 0.05$, ** $p < 0.01$ and *** $p < 0.001$ for ACP/ChOL/Se coated titanium vs pure titanium disks.*

4. Discussion

From the Figure 1 it can be observed that the deposited coating has a rose flower-like structure, which is attributed to the in situ process mechanism, as already explained in our previous research [25]. Due to the potentiostatic conditions during deposition and presence of more conductive species in the suspension used for deposition of ACP/ChOL/Se hybrid coatings, higher values of current densities are obtained, being up to 30 mA/cm^2. As explained, the hydrogen gas evolution results in the formation of pits, holes, and vacancies, creating the rose flower-like structure which can be observed in Figure 1. Nevertheless, the hybrid coating is completely covering the substrate and this coating consists of agglomerated nanoparticles. In previous research [25], it was shown that macroscale RMS value was 2.153 μm. AFM presentation of the surface morphology of the ACP/ChOL/Se hybrid coating, shown in Figure 2A proves the former statement. As it can be seen in Figure 2A, the investigated surface (scan area 1×1 μm) is relatively smooth. The linear roughness profile, presented in Figure 2B, shows root mean square roughness (RMS) value of

0.364 nm and surface roughness of 13.8 nm. This is the proof that coating condenses and agglomerates, and that the starting particles are smaller than 100 nm, which was already indicated in previous researches [15,16]. The presence of these agglomerates contributes to the formation of a rough surface, which is crucial for promoting beneficial osteoconductivity.

The homogeneity of the deposited hybrid coating's structure can be observed from EDS measurements presented in Figure 3. All the constituents, namely amorphous calcium phosphate (ACP) represented by calcium (Ca) and phosphorus (P) and selenium additive (Se), are evenly distributed across the titanium (Ti) substrate. Oxygen (O) presence is due to the polymer, oxidized titanium in the form of titanium dioxide, and the selenium salt used with the process of anodization/anaphoretic deposition process.

The XRD pattern of the ACP/ChOL/Se hybrid coating is presented in Figure 4. The XRD analysis indicates that hybrid coating exhibits characteristic wide amorphous reflection peak with maximum around 2θ=30°, suggesting that the main component of the coatings is ACP. Additionally, XRD pattern of ACP/ChOL/Se hybrid coating shows distinct diffraction peaks at 2θ=25.85° and 31.6° which correspond to (002) and (211) reflections of the HAp crystal lattice (JCPDS standard XRD card No. 86–1199). Furthermore, small peat at 2θ=46.6° and 49.6° correspond to (222) and (213) reflections of the HAp crystal lattice (JCPDS standard XRD card No. 86–1199). Reflection peak at 2θ=29.3°, as well as diffraction peaks at 2θ=35.8° and 37.4° from the enlarged section of the XRD diffractogram correspond to (213), (303) and (411) reflections of the body centered tetragonal crystal lattice of sodium selenide (JCPDS standard XRD card No. 86-1846). Due to smaller quantity of the used precursors, the former peak intensities are smaller. The XRD results confirm the transformation of amorphous ACP to crystalline HAp, ant that single-step in situ electrophoretic deposition occurs, with depositing all the species from the starting precursor solution.

The adhesion of composite coatings plays a crucial role in determining the potential biomedical applications of any composite material in the future. In order to evaluate the adhesion of ACP/ChOL/Se hybrid coatings on Ti substrate, a comprehensive adhesion test was conducted according to ASTM D 3359-02 Standard Test Methods for Measuring Adhesion by Tape, cross-cut tape test (B), given its significance for the potential medical applications of this composite material. Figure 5 shows the optical images of the ACP/ChOL/Se hybrid coating on titanium substrate after performing the adhesion test. After conducting a thorough assessment of the adhesion of the hybrid composite coating according to the ASTM D3359-02 standard, the adhesion level was determined to be 5, on a scale where 5 represents the highest adhesion (no delamination or flaking) and 0 represents the lowest adhesion (more than 65% of the coating delaminated). There is no influence of ion loading on adhesion of

the hybrid coating, since the adhesion is not affected when compared to our previous work [16].

The in vitro bioactivity of a substrate refers to its ability to form an apatite layer when exposed to biologically similar fluids. To evaluate the bioactivity of ACP/ChOL/Se hybrid coatings on titanium substrate, they were immersed in SBF solution for up to 10 days and analyzed at different time intervals. The SEM results from Figure 6 clearly demonstrate the bioactivity of ACP/ChOL/Se hybrid coating following immersion in SBF. A complete coverage of the sample surface by a new apatite layer is evident. As it can be seen in Figure 6A and 6B (Figure 6B being enlarged part of Figure 6A), even after 3 days new HAp-like layer is formed in the form of granulated agglomerates with particle sizes of few tens to 50 nm in diameter. After 10 days (Figure 6C and its enlarged part Figure 6D), it can be seen that the surface of the hybrid composite is completely covered with the newly formed apatite layer, and there is continuation of apatite growth in the form of spread across the composite surface, with continued growth of apatite in the form of granulated globular agglomerates. The formation of HAp from SBF serves as preliminary evidence for the composite-coated Ti's potential for in vivo bone bonding capability. The bone-like HAp layer formed on the implant surface after immersion in SBF is believed to support cell cascading and protein signaling, leading to the formation of new bone tissue [26]. It has been observed that this bone-like HAp layer possesses excellent osteoconductivity and exhibits a strong affinity for living bone cells [27]. Moreover, it facilitates the proliferation of osteoblast cells, promoting the generation of new bone tissue. Therefore, the development of an HAp layer along the implant material's surface is a crucial requirement for the successful osseointegration between the implant and the surrounding living bone tissue.

EDS mapping analysis results of the hybrid composites after 10 days of immersion in SBF, shown in Figure 7, confirm the bioactivity of the tested samples. Besides all the constituents (calcium (Ca), phosphorus (P), oxygen (O), selenium (Se) and titanium (Ti)), the presence of sodium (Na), magnesium (Mg), potassium (K) and chloride (Cl) was observed. Besides Ca, P and O, the later were incorporated in the top layer during immersion of samples in SBF, which is one of the proofs for bioactivity.

FTIR examination was performed on the hybrid samples before and after 10 days of immersion in SBF, and the results are shown in Figure 8. As the new apatite layer is formed, there are some changes in the bands and intensities. Since the apatite layer is grown on top, there is flattening of the weak adsorption band at around 2923 cm^{-1} which is attributed to –C-H backbone vibrations of ChOL polymer (labeled number 1 in Figure 8). Also there is enlargement and differentiation of characteristic absorption band and peak at 1633 cm^{-1} that is attributed to the OH^- of absorbed water (labeled number 2 in Figure 8) and bands that correspond to PO_4^{3-} group from ACP with distinguishable peak at 1019 cm^{-1} and two shoulders at 960 cm^{-1} and 1195 cm^{-1}

(labeled number 3. in Figure 8). Besides the HAp layer formation on top of the ACP/ChOL/Se hybrid coating during immersion in SBF, there is release of selenium ions to the medium. Hence the quantity of selenium is lowered. Therefore, the bands that correspond to sodium selenite is diminishing, which can be seen in Figure 8 as label 4. The FTIR results undoubtedly confirm the bioactivity of ACP/ChOL/Se hybrid coating on titanium substrate.

During a 28-day timeframe, the hybrid composite system underwent an observation of selenium release. Figure 9 depicts the dynamics of selenium release in a simulated body fluid (SBF) solution at 37°C under static conditions. The commonly used Peppas model [28] was employed to determine the release parameters by fitting the curve depicted in Figure 9A.

$$M_t/\mathrm{M}_\infty = kt^n,$$

The Peppas model, represented by Equation 1, was utilized to mathematically describe the kinetics of drug delivery. In this equation, $M_t/\mathrm{M}_\infty(\%)$ represents the cumulative release proportionate to the release constants k (h^{-1}) the diffusional exponent n which characterizes the release mechanism [28]. The Peppas model belongs to the category of empirical or semi-empirical mathematical models [29] that are employed to calculate the diffusional exponent n, indicating the transport mechanism.

The fitting results indicate that the release mechanism of selenium from the investigated nanocomposite biomaterials under static conditions conforms to an anomalous transport mechanism. This type of release mechanism, referred to in literature as non-Fickian transport, is observed. Notably, an increase in selenium content tends to shift the release mechanism towards Fickian diffusion. Non-Fickian transport is typically observed when a drug is released from thin polymer layers [30, 31]. The dominant phenomenon in cases of non-Fickian transport is the presence of high elastic stress in the polymer, associated with a nonlinear relaxation time [32].

Figure 9B illustrates the progression of selenium release over the course of 28 days. Following the first day (Figure 9B), the highest release rate occurs between the first and seventh day (15.8%), followed by the period between 7 and 14 days (9.5%), and finally between days 14 and 28 (8.7%). The initial higher release rate is likely attributed to the substantial amount of selenium present in the starting composite due to the synthesis procedure. Accelerated release can be observed in all systems during the first 10 days, during which 78% of the total selenium amount is released in the system.

Macrophages have an important role in the immune response to implants [33] and the presence of these cells in the tissue surrounding implants has been examined by histology or immunohistochemistry [34-38]. ACP/ChOL/Se implant has no effect on M1 cells (measured by expression of the signature molecule for these cells) at earlier time points post-implantation, which might be beneficial as inflammation in early stages is important for the prevention of infection.

However, at later time points ACP/ChOL/Se implant decreased the number of inflammatory cells suggesting better control of inflammation. Increased expression of Arg1 indicates that ACP/ChOL/Se coating results in a higher differentiation of macrophages toward the M2 phenotype which is involved in tissue repair. A higher number of M2 macrophages and increased M2/M1 ratio has been documented for some implanted materials [34,35] and attempts exist to modulate macrophage response to implant materials toward M2 phenotype [38]. In this context, a higher number of M2 cells and M2/M1 ratio might indicate that ACP/ChOL/Se coating has a beneficial effect on the immune response at the host implant interface. A lower expression of IL-1β and TNF around ACP/ChOL/Se implants indicates that selenium, although has no effect on M1 cell numbers, decreases the activity of these cells. Both IL-1β and TNF are produced by M1 macrophages [33] and are increased in response to various implanted materials [39] or titanium particles [40]. As these cytokines can activate osteoclastogenesis leading to osteolysis [40], lower levels of IL-1β and TNF induced by ACP/ChOL/Se coating might be beneficial for implant integration. In contrast to decreased IL-1β and TNF response to ACP/ChOL/Se coated disks, a transient higher IL-6 response was noted in the presence of selenium. Although decreased osteolysis was noted following prolonged (4 weeks) neutralization of IL-6 in animals [40], early and transient production might be beneficial for tissue regeneration as this cytokine is a key modulator of the inflammatory and reparative processes [41]. A lower expression of TGF-β in the tissue around ACP/ChOL/Se implants suggests reduced fibrous capsule formation in comparison to pure titanium, as a positive correlation between TGF-β and fibrosis progression has been documented [42]. Additionally, the lower expression of TGF-β might contribute to a better implantation/higher stability of ACP/ChOL/Se coated titanium into the tissue. Supporting this assumption are data showing a lower expression of this factor in the stromal cells, epithelial layers, and in vascular component in mucosa around healthy dental implants compared to failing implants [43]. Formation of novel blood vessels is also important for tissue integration of medical devices, but neovascularization has been sporadically documented in papers examining the biocompatibility of tissue implants [34–36]. VEGF is a factor involved in the regulation of angiogenesis during tissue healing, and data showing failing of dental implants in the patient under the treatment with the VEGF inhibitor [44], as well as a lower expression of this molecule in mucosa around failing implants compared to healthy implants [45], indicate an important role of VEGF in process of tissue integration. Beneficial effects of VEGF have been shown in an animal model where a higher number of endothelial cells and osteoblasts around VEGF-coated implant (compared to control implants) were noted [46]. Results we obtained indicate that ACP/ChOL/Se coating does not affect vascularization as a similar expression of VEGF was noted in the tissue around both ACP/ChOL/Se coated and pure titanium disks.

Altogether, lower inflammation and fibrosis with higher M2/M1 macrophage ratio and similar vascularization indicate that ACP/ChOL/Se coating improves implant performances and might contribute to higher stability of titanium implants.

5. Conclusions

The ACP/ChOL/Se hybrid coatings deposited on titanium substrate exhibited a rose flower-like structure, which is attributed to the in situ process mechanism. The deposition process under potentiostatic conditions and the presence of more conductive species in the suspension resulted in higher current densities during coating deposition. The hydrogen gas evolution caused the formation of pits, holes, and vacancies, creating the distinctive rose flower-like structure. However, despite the surface morphology, the hybrid coating completely covered the substrate and consisted of agglomerated nanoparticles, as confirmed by AFM analysis.

The EDS measurements demonstrated the homogeneity of the hybrid coating's structure, with all the constituents (amorphous calcium phosphate and selenium additive) evenly distributed across the titanium substrate. The XRD analysis revealed that the hybrid coating primarily consisted of amorphous calcium phosphate (ACP), with characteristic peaks corresponding to the hydroxyapatite (HAp) crystal lattice. The presence of HAp indicated the transformation of ACP to crystalline HAp during the single-step in situ electrophoretic deposition process.

The adhesion of the ACP/ChOL/Se hybrid coatings on the titanium substrate was evaluated using a tape adhesion test, which confirmed excellent adhesion with a rating of 5 on the adhesion scale. The ion loading did not significantly affect the adhesion of the hybrid coating. Furthermore, the immersion of the hybrid coatings in simulated body fluid (SBF) demonstrated their bioactivity, as evidenced by the formation of a new apatite layer on the coating surface. The SEM analysis showed the gradual growth of the apatite layer over time, indicating its potential for promoting osseointegration and bone bonding.

EDS mapping analysis confirmed the bioactivity of the samples, with additional elements such as sodium, magnesium, potassium, and chloride being incorporated into the top layer during immersion in SBF. The FTIR examination revealed changes in the absorption bands and intensities, indicating the formation of the apatite layer and the release of selenium ions to the medium.

The release dynamics of selenium from the investigated nanocomposite biomaterials were evaluated. The fitting of the release data to the Peppas model indicated an anomalous transport mechanism, characteristic of non-Fickian transport, where the release behavior deviates from traditional diffusion. The increase in selenium content led to a transition towards Fickian diffusion. The

release profiles showed an initial higher release rate, which gradually decreased over time.

ACP/ChOL/Se implant has no effect on M1 cells (macrophages) at earlier time points post-implantation, which might be beneficial as inflammation in early stages is important for the prevention of infection. At the same time, it was found to be increased Arg1 and M2/M1 ratio expression which might indicate that coating has a beneficial effect on the immune response at the host implant interface. A lower inflammatory mediators (IL-1β and TNF) expression around ACP/ChOL/Se implants indicates that selenium might be beneficial for implant integration. A transient higher IL-6 response (key modulator of the inflammatory and reparative processes) was noted in the presence of selenium, and early and transient production might be beneficial for tissue regeneration. A lower expression of TGF-β in the tissue around ACP/ChOL/Se implants suggests reduced fibrous capsule formation in comparison to pure titanium. Hence, the lower expression of transforming growth factor (TGF-β) might contribute to a better implantation/higher stability of ACP/ChOL/Se coated titanium into the tissue. Obtained results indicate that ACP/ChOL/Se coating does not affect vascularization. Lower inflammation and fibrosis with higher M2/M1 macrophage ratio and similar vascularization indicate that ACP/ChOL/Se coating improves implant performances and might contribute to higher stability of titanium implants.

Overall, the ACP/ChOL/Se hybrid coatings exhibited favorable characteristics for potential biomedical applications. Their excellent adhesion, bioactivity, and controlled release behavior make them promising candidates for orthopedic implants and other medical devices. Further studies are warranted to assess their long-term stability, cytocompatibility, and corrosion performance.

Acknowledgements: This work was supported by the Ministry of Science, Technological Development and Innovation of the Republic of Serbia (Grant No. 451-03-47/2023-01/200026, grant No. 451-03-47/2023-01/200175 and grant No. 451–03–47/2023–01/200007).

References

1. Williams, D.F. Titanium for Medical Applications BT - Titanium in Medicine: Material Science, Surface Science, Engineering, Biological Responses and Medical Applications. In; Brunette, D.M., Tengvall, P., Textor, M., Thomsen, P., Eds.; Springer Berlin Heidelberg: Berlin, Heidelberg, 2001; pp. 13–24 ISBN 978-3-642-56486-4.
2. Ripamonti, U.; Roden, L.C.; Renton, L.F. Osteoinductive Hydroxyapatite-Coated Titanium Implants. *Biomaterials* **2012**, *33*, 3813–3823, doi:10.1016/j.biomaterials.2012.01.050.

3. de Lange, G.L.; Donath, K. Interface between Bone Tissue and Implants of Solid Hydroxyapatite or Hydroxyapatite-Coated Titanium Implants. *Biomaterials* **1989**, *10*, 121–125, doi:https://doi.org/10.1016/0142-9612(89)90044-6.
4. Meirelles, L.; Arvidsson, A.; Andersson, M.; Kjellin, P.; Albrektsson, T.; Wennerberg, A. Nano Hydroxyapatite Structures Influence Early Bone Formation. *J. Biomed. Mater. Res. Part A* **2008**, *87A*, 299–307, doi:https://doi.org/10.1002/jbm.a.31744.
5. Dorozhkin, S. V. Synthetic Amorphous Calcium Phosphates (ACPs): Preparation, Structure, Properties, and Biomedical Applications. *Biomater. Sci.* **2021**, *9*, 7748–7798, doi:10.1039/D1BM01239H.
6. Akshaya, S.; Rowlo, P.K.; Dukle, A.; Nathanael, A.J. Antibacterial Coatings for Titanium Implants: Recent Trends and Future Perspectives. *Antibiotics* 2022, *11*, doi:10.3390/antibiotics11121719.
7. Chen, X.; Zhou, J.; Qian, Y.; Zhao, L. Antibacterial Coatings on Orthopedic Implants. *Mater. Today Bio* **2023**, *19*, 100586, doi:https://doi.org/10.1016/j.mtbio.2023.100586.
8. Trujillo, N.A.; Floreani, R.; Ma, H.; Bryers, J.D.; Williams, J.D.; Popat, K.C. Antibacterial Effects of Silver-Doped Hydroxyapatite Thin Films Sputter Deposited on Titanium. *Mater. Sci. Eng. C* **2012**, *32*, 2135–2144, doi:https://doi.org/10.1016/j.msec.2012.05.012.
9. Zhang, K.; Zhang, B.; Huang, C.; Gao, S.; Li, B.; Cao, R.; Cheng, J.; Li, R.; Yu, Z.; Xie, X. Biocompatibility and Antibacterial Properties of Pure Titanium Surfaces Coated with Yttrium-Doped Hydroxyapatite. *J. Mech. Behav. Biomed. Mater.* **2019**, *100*, 103363, doi:https://doi.org/10.1016/j.jmbbm.2019.07.021.
10. Li, Q.; Song, S.; Li, J.; Yang, J.; Zhang, R.; Niinomi, M.; Nakano, T. Antibacterial Properties and Biocompatibility of Hydroxyapatite Coating Doped with Various Cu Contents on Titanium. *Mater. Trans.* **2022**, *63*, 1072–1079, doi:10.2320/matertrans.MT-M2021245.
11. Geng, Z.; Wang, R.; Zhuo, X.; Li, Z.; Huang, Y.; Ma, L.; Cui, Z.; Zhu, S.; Liang, Y.; Liu, Y.; et al. Incorporation of Silver and Strontium in Hydroxyapatite Coating on Titanium Surface for Enhanced Antibacterial and Biological Properties. *Mater. Sci. Eng. C* **2017**, *71*, 852–861, doi:https://doi.org/10.1016/j.msec.2016.10.079.
12. Liu, Y.-C.; Lee, Y.-T.; Huang, T.-C.; Lin, G.-S.; Chen, Y.-W.; Lee, B.-S.; Tung, K.-L. In Vitro Bioactivity and Antibacterial Activity of Strontium-, Magnesium-, and Zinc-Multidoped Hydroxyapatite Porous Coatings Applied via Atmospheric Plasma Spraying. *ACS Appl. Bio Mater.* **2021**, *4*, 2523–2533, doi:10.1021/acsabm.0c01535.
13. Li, J.; Zhuang, S. Antibacterial Activity of Chitosan and Its Derivatives and Their Interaction Mechanism with Bacteria: Current State and

Perspectives. *Eur. Polym. J.* **2020**, *138*, 109984, doi:10.1016/j.eurpolymj.2020.109984.
14. Li, B.; Xia, X.; Guo, M.; Jiang, Y.; Li, Y.; Zhang, Z.; Liu, S.; Li, H.; Liang, C.; Wang, H. Biological and Antibacterial Properties of the Micro-Nanostructured Hydroxyapatite/Chitosan Coating on Titanium. *Sci. Rep.* **2019**, *9*, 14052, doi:10.1038/s41598-019-49941-0.
15. Pantović Pavlović, M.R.; Stanojević, B.P.; Pavlović, M.M.; Mihailović, M.D.; Stevanović, J.S.; Panić, V. V; Ignjatović, N.L. Anodizing/Anaphoretic Electrodeposition of Nano-Calcium Phosphate/Chitosan Lactate Multifunctional Coatings on Titanium with Advanced Corrosion Resistance, Bioactivity, and Antibacterial Properties. *ACS Biomater. Sci. Eng.* **2021**, *7*, 3088–3102, doi:10.1021/acsbiomaterials.1c00035.
16. Pantović Pavlović, M.R.; Pavlović, M.M.; Eraković, S.; Stevanović, J.S.; Panić, V. V; Ignjatović, N. Simultaneous Anodization/Anaphoretic Electrodeposition Synthesis of Nano Calcium Phosphate/Titanium Oxide Composite Coatings Assisted with Chitosan Oligosaccharide Lactate. *Mater. Lett.* **2020**, *261*, 127121, doi:https://doi.org/10.1016/j.matlet.2019.127121.
17. Stevanović, M.; Djošić, M.; Janković, A.; Kojić, V.; Stojanović, J.; Grujić, S.; Bujagić, I.M.; Rhee, K.Y.; Mišković-Stanković, V. The Chitosan-Based Bioactive Composite Coating on Titanium. *J. Mater. Res. Technol.* **2021**, *15*, 4461–4474, doi:https://doi.org/10.1016/j.jmrt.2021.10.072.
18. Zhong, Z.; Qin, J.; Ma, J. Cellulose Acetate/Hydroxyapatite/Chitosan Coatings for Improved Corrosion Resistance and Bioactivity. *Mater. Sci. Eng. C* **2015**, *49*, 251–255, doi:https://doi.org/10.1016/j.msec.2015.01.020.
19. Rath, P.C.; Singh, B.P.; Besra, L.; Bhattacharjee, S. Multiwalled Carbon Nanotubes Reinforced Hydroxyapatite-Chitosan Composite Coating on Ti Metal: Corrosion and Mechanical Properties. *J. Am. Ceram. Soc.* **2012**, *95*, 2725–2731, doi:https://doi.org/10.1111/j.1551-2916.2012.05195.x.
20. Chandorkar, Y.; K, R.; Basu, B. The Foreign Body Response Demystified. *ACS Biomater. Sci. Eng.* **2019**, *5*, 19–44, doi:10.1021/acsbiomaterials.8b00252.
21. Lebaudy, E.; Fournel, S.; Lavalle, P.; Vrana, N.E.; Gribova, V. Recent Advances in Antiinflammatory Material Design. *Adv. Healthc. Mater.* **2021**, *10*, 2001373, doi:https://doi.org/10.1002/adhm.202001373.
22. Toy, V.E.; Dundar, S.; Bozoglan, A. The Effects of a Nonsteroidal Anti-Inflammatory Drug on the Degree of Titanium Implant Osseointegration. *J. Oral Biol. Craniofacial Res.* **2020**, *10*, 333–336, doi:https://doi.org/10.1016/j.jobcr.2020.06.006.

23. Salduz, A.; Dikici, F.; Kılıçoğlu, Ö.I.; Balcı, H.I.; Akgul, T.; Kürkçü, M.; Kurtoğlu, C.; Tözün, R. Effects of NSAIDs and Hydroxyapatite Coating on Osseointegration: Biomechanical and Histological Study on Rabbits. *J. Orthop. Surg.* **2017**, *25*, 2309499016684410, doi:10.1177/2309499016684410.
24. Li, L.; Yu, M.; Li, Y.; Li, Q.; Yang, H.; Zheng, M.; Han, Y.; Lu, D.; Lu, S.; Gui, L. Synergistic Anti-Inflammatory and Osteogenic n-HA/Resveratrol/Chitosan Composite Microspheres for Osteoporotic Bone Regeneration. *Bioact. Mater.* **2021**, *6*, 1255–1266, doi:https://doi.org/10.1016/j.bioactmat.2020.10.018.
25. Pantović Pavlović, M.R.; Ignjatović, N.L.; Panić, V. V; Mirkov, I.I.; Kulaš, J.B.; Malešević, A.L.; Pavlović, M.M. Immunomodulatory Effects Mediated by Nano Amorphous Calcium Phosphate/Chitosan Oligosaccharide Lactate Coatings Decorated with Selenium on Titanium Implants. *J. Funct. Biomater.* 2023, *14*.
26. Kokubo, T.; Kim, H.M.; Kawashita, M.; Nakamura, T. Bioactive Metals: Preparation and Properties. *J. Mater. Sci. Mater. Med.* **2004**, *15*, 99–107, doi:10.1023/B:JMSM.0000011809.36275.0c.
27. Kumar, A.M.; Suresh, B.; Das, S.; Obot, I.B.; Adesina, A.Y.; Ramakrishna, S. Promising Bio-Composites of Polypyrrole and Chitosan: Surface Protective and in Vitro Biocompatibility Performance on 316L SS Implants. *Carbohydr. Polym.* **2017**, *173*, 121–130, doi:https://doi.org/10.1016/j.carbpol.2017.05.083.
28. Ritger, P.L.; Peppas, N.A. A Simple Equation for Description of Solute Release I. Fickian and Non-Fickian Release from Non-Swellable Devices in the Form of Slabs, Spheres, Cylinders or Discs. *J. Control. Release* **1987**, *5*, 23–36, doi:https://doi.org/10.1016/0168-3659(87)90034-4.
29. Siepmann, J.; Siepmann, F. Mathematical Modeling of Drug Delivery. *Int. J. Pharm.* **2008**, *364*, 328–343, doi:https://doi.org/10.1016/j.ijpharm.2008.09.004.
30. Saettone, M.F.; Chetoni, P.; Bianchi, L.M.; Giannaccini, B.; Conte, U.; Sangalli, M.E. Controlled Release of Timolol Maleate from Coated Ophthalmic Mini-Tablets Prepared by Compression. *Int. J. Pharm.* **1995**, *126*, 79–82, doi:https://doi.org/10.1016/0378-5173(95)04096-X.
31. Hasimi, A.; Stavropoulou, A.; Papadokostaki, K.G.; Sanopoulou, M. Transport of Water in Polyvinyl Alcohol Films: Effect of Thermal Treatment and Chemical Crosslinking. *Eur. Polym. J.* **2008**, *44*, 4098–4107, doi:https://doi.org/10.1016/j.eurpolymj.2008.09.011.
32. Edwards, D.A. Non-Fickian Diffusion in Thin Polymer Films. *J. Polym. Sci. Part B Polym. Phys.* **1996**, *34*, 981–997, doi:https://doi.org/10.1002/(SICI)1099-0488(19960415)34:5<981::AID-POLB16>3.0.CO;2-7.

33. Kzhyshkowska, J.; Gudima, A.; Riabov, V.; Dollinger, C.; Lavalle, P.; Vrana, N.E. Macrophage Responses to Implants: Prospects for Personalized Medicine. *J. Leukoc. Biol.* **2015**, *98*, 953–962, doi:10.1189/jlb.5VMR0415-166R.
34. Muhamed, J.; Revi, D.; Rajan, A.; Geetha, S.; Anilkumar, T. V Biocompatibility and Immunophenotypic Characterization of a Porcine Cholecyst-Derived Scaffold Implanted in Rats. *Toxicol. Pathol.* **2015**, *43*, 536–545, doi:10.1177/0192623314550722.
35. Muhamed, J.; Revi, D.; Rajan, A.; Anilkumar, T. V Comparative Local Immunogenic Potential of Scaffolds Prepared from Porcine Cholecyst, Jejunum, and Urinary Bladder in Rat Subcutaneous Model. *J. Biomed. Mater. Res. B. Appl. Biomater.* **2015**, *103*, 1302–1311, doi:10.1002/jbm.b.33296.
36. Barbeck, M.; Alkildani, S.; Mandlule, A.; Radenković, M.; Najman, S.; Stojanović, S.; Jung, O.; Ren, Y.; Cai, B.; Görke, O.; et al. In Vivo Analysis of the Immune Response to Strontium- and Copper-Doped Bioglass. *In Vivo* **2022**, *36*, 2149–2165, doi:10.21873/invivo.12941.
37. Lužajić Božinovski, T.; Todorović, V.; Milošević, I.; Prokić, B.B.; Gajdov, V.; Nešović, K.; Mišković-Stanković, V.; Marković, D. Macrophages, the Main Marker in Biocompatibility Evaluation of New Hydrogels after Subcutaneous Implantation in Rats. *J. Biomater. Appl.* **2022**, *36*, 1111–1125, doi:10.1177/08853282211046119.
38. Hachim, D.; LoPresti, S.T.; Rege, R.D.; Umeda, Y.; Iftikhar, A.; Nolfi, A.L.; Skillen, C.D.; Brown, B.N. Distinct Macrophage Populations and Phenotypes Associated with IL-4 Mediated Immunomodulation at the Host Implant Interface. *Biomater. Sci.* **2020**, *8*, 5751–5762, doi:10.1039/D0BM00568A.
39. Perala, D.G.; Chapman, R.J.; Gelfand, J.A.; Callahan, M. V; Adams, D.F.; Lie, T. Relative Production of IL-1β and TNFα by Mononuclear Cells After Exposure to Dental Implants. *J. Periodontol.* **1992**, *63*, 426–430, doi:10.1902/jop.1992.63.5.426.
40. Eger, M.; Hiram-Bab, S.; Liron, T.; Sterer, N.; Carmi, Y.; Kohavi, D.; Gabet, Y. Mechanism and Prevention of Titanium Particle-Induced Inflammation and Osteolysis. *Front. Immunol.* **2018**, *9*, 2963, doi:10.3389/fimmu.2018.02963.
41. Johnson, B.Z.; Stevenson, A.W.; Prêle, C.M.; Fear, M.W.; Wood, F.M. The Role of IL-6 in Skin Fibrosis and Cutaneous Wound Healing. *Biomedicines* **2020**, *8*, doi:10.3390/biomedicines8050101.
42. Park, C.; Lee, S.-W.; Kim, J.; Song, E.-H.; Jung, H.-D.; Park, J.-U.; Kim, H.-E.; Kim, S.; Jang, T.-S. Reduced Fibrous Capsule Formation at Nano-Engineered Silicone Surfaces via Tantalum Ion Implantation. *Biomater. Sci.* **2019**, *7*, 2907–2919, doi:10.1039/C9BM00427K.

43. Cornelini, R.; Rubini, C.; Fioroni, M.; Favero, G.A.; Strocchi, R.; Piattelli, A. Transforming Growth Factor-Beta 1 Expression in the Peri-Implant Soft Tissues of Healthy and Failing Dental Implants. *J. Periodontol.* **2003**, *74*, 446–450, doi:10.1902/jop.2003.74.4.446.
44. Emami, E.; de Grandmont, P.; Menassa, M.; Audy, N.; Durand, R. Anti-Vascular Endothelial Growth Factors as a Potential Risk for Implant Failure: A Clinical Report. *Case Rep. Med.* **2020**, *2020*, 6141493.
45. Cornelini, R.; Artese, L.; Rubini, C.; Fioroni, M.; Ferrero, G.; Santinelli, A.; Piattelli, A. Vascular Endothelial Growth Factor and Microvessel Density around Healthy and Failing Dental Implants. *Int. J. Oral Maxillofac. Implants* **2001**, *16*, 389–393.
46. Guang, M.; Huang, B.; Yao, Y.; Zhang, L.; Yang, B.; Gong, P. Effects of Vascular Endothelial Growth Factor on Osteoblasts around Dental Implants in Vitro and in Vivo. *J. Oral Sci.* **2017**, *59*, 215–223, doi:10.2334/josnusd.16-0406.